Module - 4 Incompressible Flows over Finite Wings

Biot-Savart law and Helmholtz's theorems, Vortex filament: Infinite and semi-infinite vortex filament, Induced velocity. Prandtl's classical lifting line theory: Downwash and induced drag. Elliptical and modified elliptical lift distribution. Lift distribution on wings. Limitations of Prandtl's lifting line theory. Extended lifting line theory- lifting surface theory, vortex lattice method for wings. Lift, drag and moment characteristics of complete airplane.

Downwash and Induced drag:

A finite wing is a three-dimensional body, and consequently the flow over the finite wing is three-dimensional; that is, there is a component of flow in the spanwise direction. To see this more clearly, examine Figure 2.1, which gives the top and front views of a finite wing. The physical mechanism for generating lift on the wing is the existence of a high pressure on the bottom surface and a low pressure on the top surface. The net imbalance of the pressure distribution creates the lift. However, as a by-product of this pressure imbalance, the flow near the wing tips tends to curl around the tips, being forced from the high-pressure region just underneath the tips to the low-pressure region on top. This flow around the wing tips is shown in the front view of the wing in Figure 2.1. As a result, on the top surface of the wing, there is generally a spanwise component of flow from the tip toward the wing root, causing the streamlines over the top surface to bend toward the root, as sketched on the top view shown in Figure 2.1. Similarly, on the bottom surface of the wing, there is generally a spanwise component of flow from the root toward the tip, causing the streamlines over the bottom surface to bend toward the tip. Clearly, the flow over the finite wing is three-dimensional.

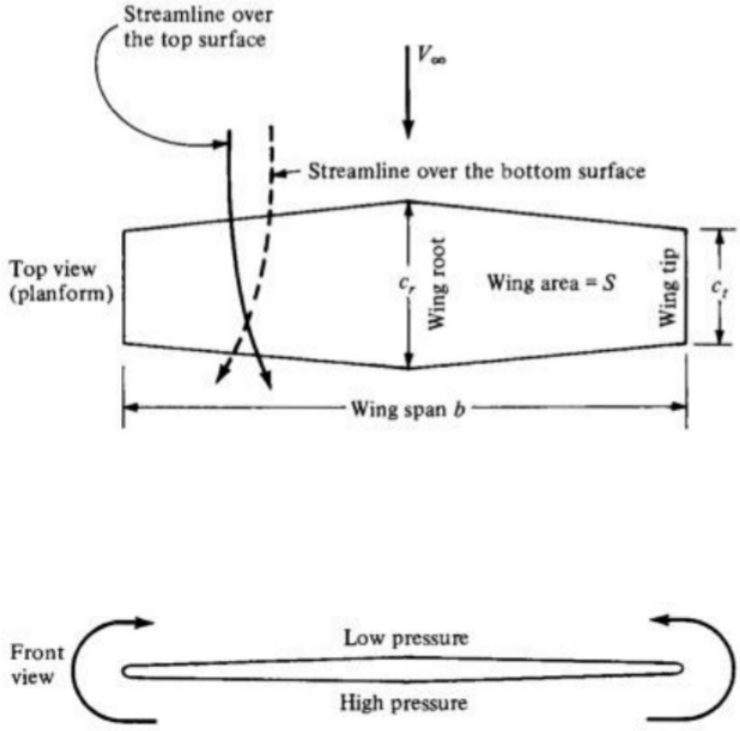

Figure 2.1 Finite wing. In this figure, the curvature of the streamlines over the top and bottom of the wing is exaggerated for clarity.

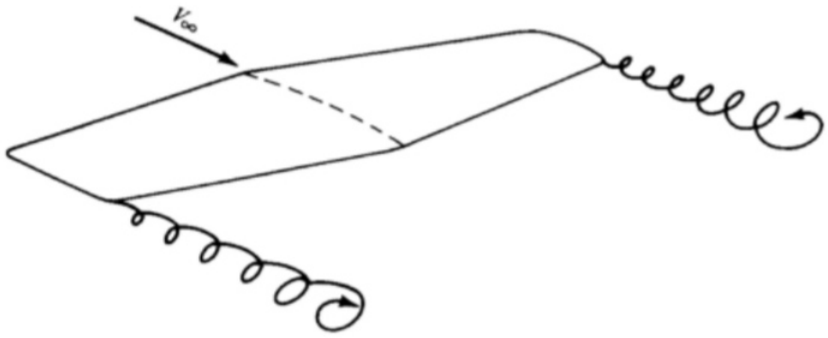

Figure 2.2 Schematic of wing-tip vortices

The tendency for the flow to "leak" around the wing tips has another important effect on the aerodynamics of the wing. This flow establishes a circulatory motion that trails downstream of the wing; that is, a trailing *vortex* is created at each wing tip. These wing-tip vortices are sketched in Figure 2.2. The tip vortices are essentially weak "tornadoes" that trail downstream of the finite wing. These wing-tip vortices downstream of the wing induce a small downward component of air velocity in the neighbourhood of the wing itself. The two vortices tend to drag the surrounding air around with them, and this secondary movement induces a small velocity component in the downward direction at the wing. This downward component is called *downwash,* denoted by the symbol *w*. In turn, the downwash combines with the freestream velocity V_∞ to produce a *local* relative wind which is canted downward in the vicinity of each airfoil section of the wing, as sketched in Figure 2.3.

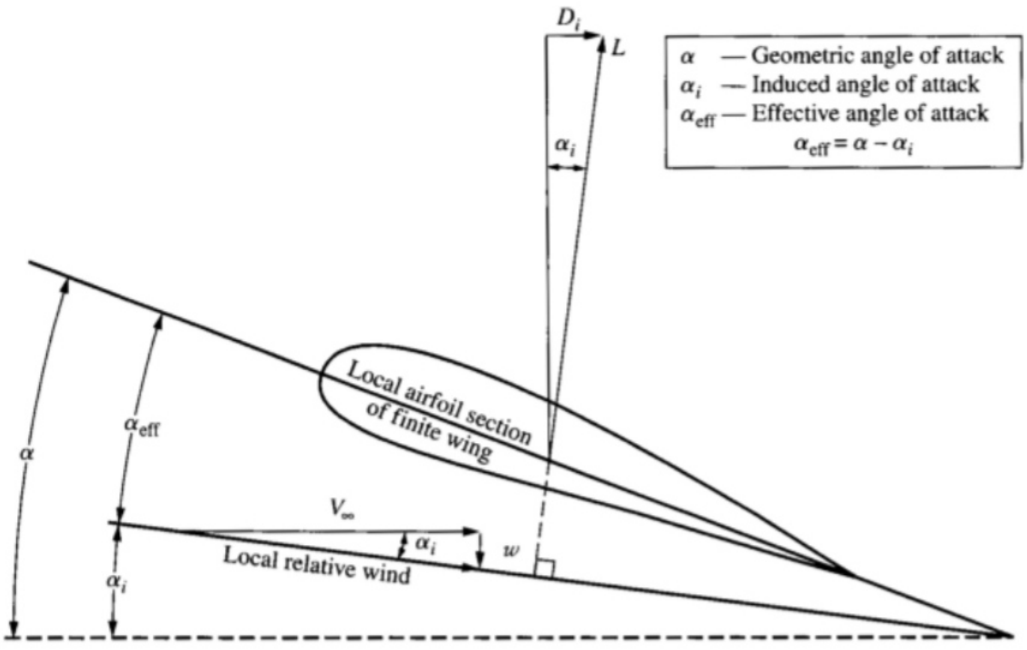

Figure 2.3 Effect of downwash on the local flow over a local airfoil section of a finite wing.

Examine Figure 2.3 closely. The angle between the chord line and the direction of V_∞ is the angle of attack α. We now more precisely define α *as* the *geometric* angle of attack. In Figure 2.3, the local relative wind is inclined below the direction of V_∞ by the angle α_i, called the *induced* angle of attack. The presence of downwash, and its effect on inclining the local

relative wind in the downward direction, has two important effects on the local airfoil section, as follows:

1. The angle of attack actually seen by the local airfoil section is the angle between the chord line and the local relative wind. This angle is given by α_{eff} in Figure 2.3 and is defined as the *effective* angle of attack. Hence, although the wing is at a geometric angle of attack α, the local airfoil section is seeing a smaller angle, namely, the effective angle of attack α_{eff}. From Figure 2.3,

$$\alpha_{\text{eff}} = \alpha - \alpha_i \tag{2.1}$$

2. The local lift vector is aligned perpendicular to the local relative wind, and hence is inclined behind the vertical by the angle α_i, as shown in Figure 2.3. Consequently, there is a component of the local lift vector in the direction of V_∞ that is, there is a *drag* created by the presence of downwash. This drag is defined as *induced drag,* denoted by D_i in Figure 2.3.

Hence, we see that the presence of downwash over a finite wing reduces the angle of attack that each section effectively sees, and moreover, it creates a component of drag-the induced drag D_i.

The tilting backward of the lift vector shown in Figure 2.3 is one way of visualizing the physical generation of induced drag. Two alternate ways are as follows:

1. The three-dimensional flow induced by the wing-tip vortices shown in Figure 2.2 simply alters the pressure distribution on the finite wing in such a fashion that a net pressure imbalance exists in the direction of V_∞ (i.e., drag is created). In this sense, induced drag is a type of "pressure drag."
2. The wing-tip vortices contain a large amount of translational and rotational kinetic energy. This energy has to come from somewhere; indeed, it is ultimately provided by the aircraft engine, which is the only source of power associated with the airplane. Since the energy of the vortices serves no useful purpose, this power is essentially lost. In effect, the extra power provided by the engine that goes into the vortices is the extra power required from the engine to overcome the induced drag.

The vortex filament, The Biot-Savart Law, And Helmholtz's Theorems:

The concept of a vortex filament first introduced in Unit 1. In general, a vortex filament can be *curved,* as shown in Figure 2.4. Here, only a portion of the filament is illustrated.

The filament induces a flow field in the surrounding space. If the circulation is taken about any path enclosing the filament, a constant value Γ is obtained. Hence, the strength of the vortex filament is defined as Γ. Consider a directed segment of the filament **dl,** as shown in Figure 2.4. The radius vector from **dl** to an arbitrary point P in space is **r.** The segment **dl** induces a velocity at *P* equal to

$$\boxed{\mathbf{dV} = \frac{\Gamma}{4\pi} \frac{\mathbf{dl} \times \mathbf{r}}{|\mathbf{r}|^3}} \tag{2.2}$$

Equation (2.2) is called the *Biot-Savart law* and is one of the most fundamental relations in the theory of inviscid, incompressible flow.

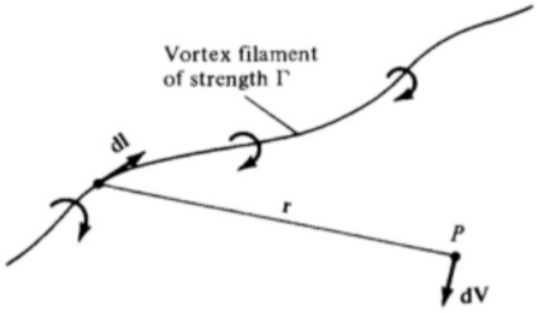

Figure 2.4 Vortex filament and illustration of the Biot-Savart law.

Let us apply the Biot-Savart law to a straight vortex filament of infinite length, as sketched in Figure 2.5. The strength of the filament isΓ. The velocity induced at point *P* by the directed segment of the vortex filament *dl* is given by Equation (2.2). Hence, the velocity induced at *P* by the entire vortex filament is

$$\mathbf{V} = \int_{-\infty}^{\infty} \frac{\Gamma}{4\pi} \frac{\mathbf{dl} \times \mathbf{r}}{|\mathbf{r}|^3} \tag{2.3}$$

From the definition of the vector cross product, the direction of **V** is downward in Figure 2.5. The magnitude of the velocity, $V = |\mathbf{V}|$, is given by

$$V = \frac{\Gamma}{4\pi} \int_{-\infty}^{\infty} \frac{\sin\theta}{r^2} dl \tag{2.4}$$

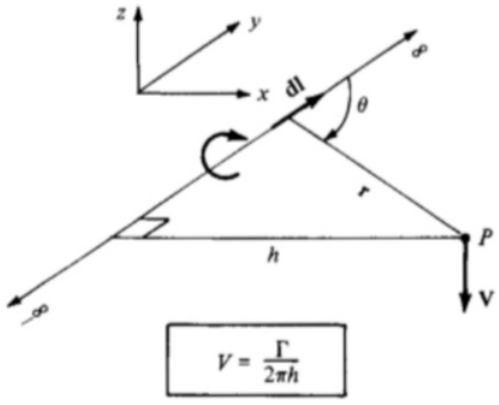

Figure 2.5 velocity induced at point P by an infinite, straight vortex filament

In Figure 2.5, let *h* be the perpendicular distance from point *P* to the vortex filament. Then, from the geometry shown in figure 2.5,

$$r = \frac{h}{\sin\theta}$$

$$l = \frac{h}{\tan\theta}$$

$$dl = -\frac{h}{\sin^2\theta} d\theta \tag{2.5}$$

Subsituting Equation (2.5) in Equation (2.4), we have

$$V = \frac{\Gamma}{4\pi}\int_{-\infty}^{\infty}\frac{\sin\theta}{r^2}dl = -\frac{\Gamma}{4\pi h}\int_{\pi}^{0}\sin\theta\, d\theta$$

$$V = \frac{\Gamma}{2\pi h} \tag{2.6}$$

Thus, the velocity induced at a given point P by an infinite, straight vortex filament at a perpendicular distance h from P is simply $\Gamma/2\pi h$.

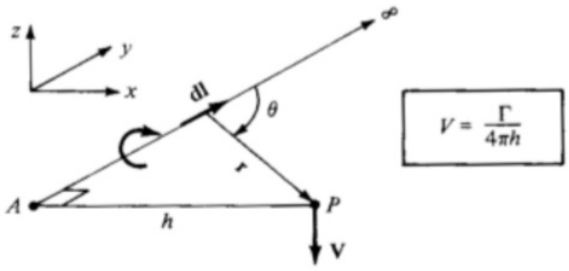

Figure 2.6 velocity induced at point P by an semi-infinite, straight vortex filament

Consider the semi-infinite vortex filament shown in Figure 2.6. The filament extends from point A to ∞. Point A can be considered a boundary of the flow. Let P be a point in the plane through A perpendicular to the filament. Then, by an integration similar to that above, the velocity induced at P by the semi-infinite vortex filament is

$$V = \frac{\Gamma}{4\pi h} \tag{2.7}$$

Helmholtz's vortex theorems states:

1. The strength of a vortex filament is constant along its length.
2. A vortex filament cannot end in a fluid; it must extend to the boundaries of the fluid (which can be $\pm\infty$) or form a closed path.

Prandtl's lifting line theory and its limitations:

The first practical theory for predicting the aerodynamic properties of a finite wing was developed by Ludwig Prandtl and his colleagues at Gottingen, Germany, during the period 1911-1918, spanning World War I. The utility of Prandtl's theory is so great that it is still in use today for preliminary calculations of finite-wing characteristics. The purpose of this section is to describe Prandtl's theory and to lay the groundwork for the modem numerical methods.

Prandtl reasoned as follows. A vortex filament of strength r that is somehow bound to a fixed location in a flow so called bound vortex will experience a force $L' = \rho_\infty V_\infty \Gamma$ from the Kutta-Joukowski theorem. This bound vortex is in contrast to a *free vortex,* which moves with the same fluid elements throughout a flow. Therefore, let us replace a finite wing of span b with a bound vortex, extending from $y = -b/2$ to $y = b/2$, as sketched in Figure 2.7. However, due to Helmholtz's theorem, a vortex filament cannot end in the fluid. Therefore, assume the vortex filament continues as two free vortices trailing downstream from the wing

tips to infinity, as also shown in Figure 2.7. This vortex (the bound plus the two free) is in the shape of a horseshoe, and therefore is called a *horseshoe vortex.*

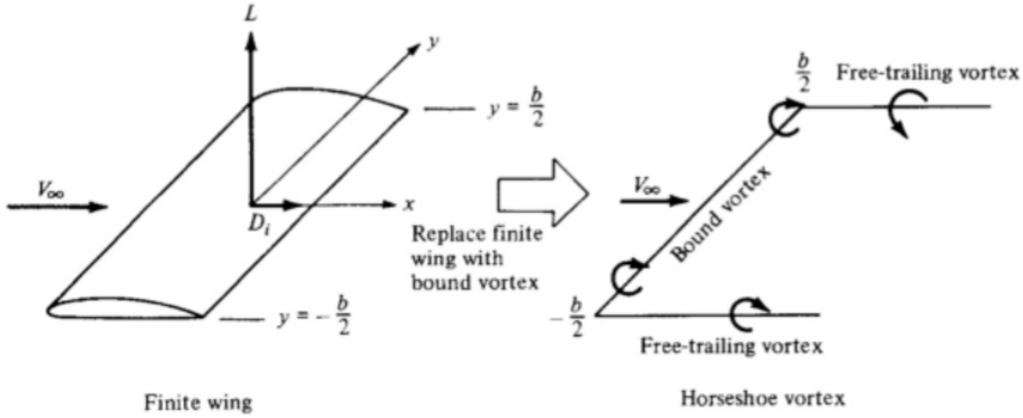

Figure 2.7 replacement of the finite wing with a bound vortex

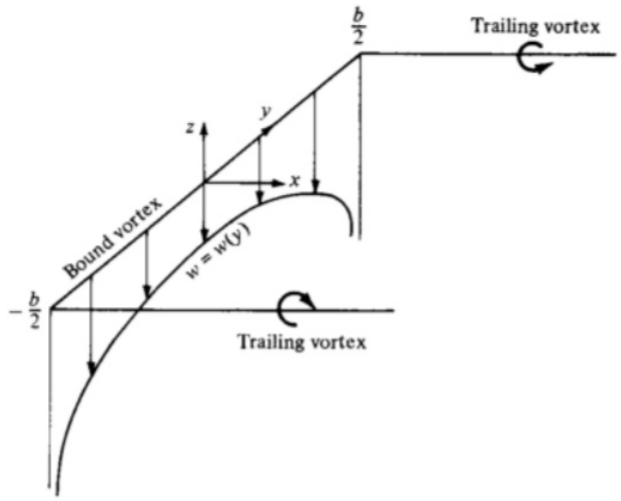

Figure 2.8 Downwash distribution along the y axis for a single horseshoe vortex

A single horseshoe vortex is shown in Figure 2.8. Consider the downwash *w* induced along the bound vortex from -*b* /2 to *b* /2 by the horseshoe vortex. Examining Figure 2.8, we see that the bound vortex induces no velocity along itself; however, the two trailing vortices both contribute to the induced velocity along the bound vortex, and both contributions are in the downward direction. Consistent with the *xyz* coordinate system in Figure 2.8, such a downward velocity is negative; that is, *w* (which is in the *z* direction) is a negative value when directed downward and a positive value when directed upward. If the origin is taken at the center of the bound vortex, then the velocity at any point y along the bound vortex induced by the trailing semi-infinite vortices is, from Equation (2.7),

$$w(y) = -\frac{\Gamma}{4\pi(b/2 + y)} - \frac{\Gamma}{4\pi(b/2 - y)} \tag{2.8}$$

In Equation (2.8), the first term on the right-hand side is the contribution from the left trailing vortex (trailing from -*b* /2), and the second term is the contribution from the right trailing vortex (trailing from b/2). Equation (2.8) reduces to

$$w(y) = -\frac{\Gamma}{4\pi}\frac{b}{(b/2)^2 - y^2} \tag{2.9}$$

This variation of *w(y)* is sketched in Figure 2.8. Note that *w* approaches -∞ as *y* approaches *-b/2* or *b/2*.

Limitations:

The downwash distribution due to the single horseshoe vortex shown in Figure 2.8 does not realistically simulate that of a finite wing; the downwash approaching an infinite value at the tips is especially disconcerting

Fundamental Equation of Prandtl's lifting-line theory:

Let us superimpose a large number of horseshoe vortices, each with a different length of the bound vortex, but with all the bound vortices coincident along a single line, called the *lifting line.* This concept is illustrated in Figure 2.9, where only three horseshoe vortices are shown for the sake of clarity. In Figure 2.9, a horseshoe vortex of strength $d\Gamma_1$ is shown, where the bound vortex spans the entire wing from *-b* /2 to *b* /2 (from point *A* to point *F).* *S*uperimposed on this is a second horseshoe vortex of strength $d\Gamma_2$ where its bound vortex spans only part of the wing, from point *B* to point *E.* Finally, superimposed on this is a third horseshoe vortex of strength $d\Gamma_3$, where its bound vortex spans only the part of the wing from point *C* to point *D.* As a result, the circulation varies along the line of bound vortices-the lifting line defined above. Along *AB* and *EF,* where only one vortex is present, the circulation is $d\Gamma_1$. However, along *BC* and *DE,* where two vortices are superimposed, the circulation is the sum of their strengths $d\Gamma_1 + d\Gamma_2$. Along *c D,* three vortices are superimposed, and hence the circulation is $d\Gamma_1 + d\Gamma_2 + d\Gamma_3$. The series of trailing vortices in Figure 2.9 represents pairs of vortices, each pair associated with a given horseshoe vortex. Note that the strength of each trailing vortex is equal to the *change in circulation* along the lifting line.

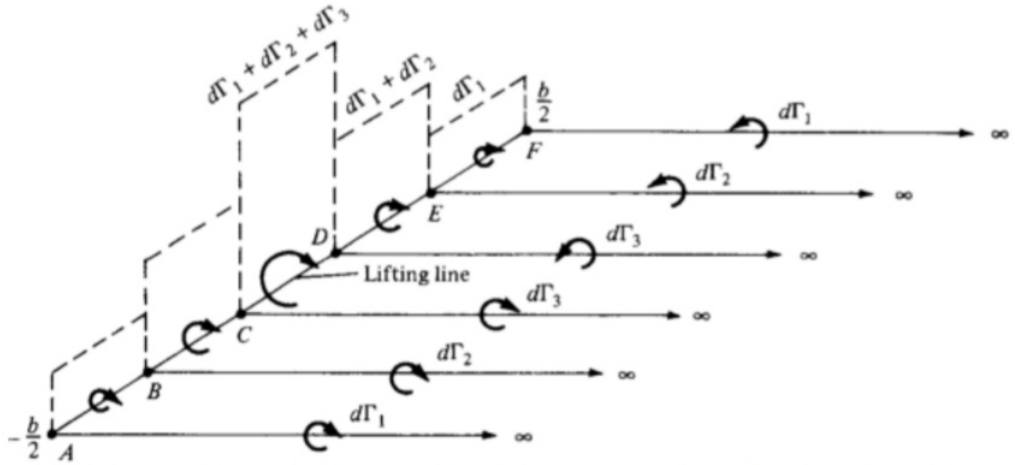

Figure 2.9 Superposition of a finite number of horseshoe vortices along the lifting line.

Let us extrapolate Figure 2.9 to the case where an *infinite number* of horseshoe vortices are superimposed along the lifting line, each with a vanishingly small strength $d\Gamma$, This case is illustrated in Figure 2.10. Note that the vertical bars in Figure 2.9 have now become a continuous distribution of $\Gamma(y)$ along the lifting line in Figure 2.10. The value of the

circulation at the origin is Γ_0. Also, note that the finite number of trailing vortices in Figure 2.9 have become a *continuous vortex sheet* trailing downstream of the lifting line in Figure 2.10. This vortex sheet is parallel to the direction of V_∞. The total strength of the sheet integrated across the span of the wing is zero, because it consists of pairs of trailing vortices of equal strength but in opposite directions.

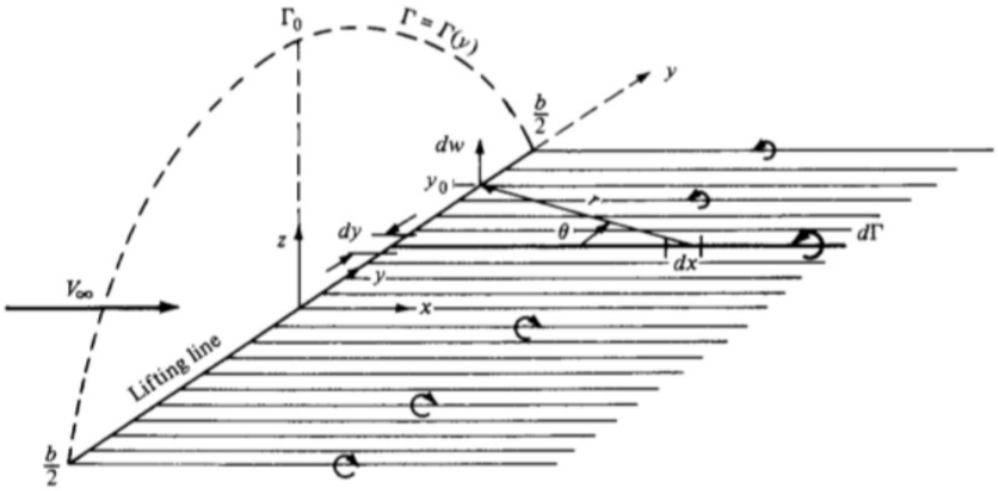

Figure 2.10 Superposition of a infinite number of horseshoe vortices along the lifting line.

Let us single out an infinitesimally small segment of the lifting line *dy* located at the coordinate *y* as shown in Figure 2.10. The circulation at *y* is Γ(y), and the change in circulation over the segment *dy* is $d\Gamma = (d\Gamma/dy)\,dy$. Consider more closely the trailing vortex of strength $d\Gamma$ which intersects the lifting line at coordinate *y,* as shown in Figure 2.10. Also consider the arbitrary location y_0 along the lifting line. Any segment of the trailing vortex *dx* will induce a velocity at y_0 with a magnitude and direction given by the Biot-Savart law, Equation (2.2). In tum, the velocity *dw* at y_0 induced by the entire semi-infinite trailing vortex located at *y* is given by Equation (2.7), which in terms of the picture given in Figure 2.10 yields

$$dw = -\frac{(d\Gamma/dy)\,dy}{4\pi(y_0 - y)} \tag{2.10}$$

[The minus sign in Equation (2.10) is needed for consistency with the picture shown in Figure 2.10; for the trailing vortex shown, the direction of *d w* at y_0 is upward and hence is a positive value, whereas Γ is decreasing in the *y* direction, making $d\Gamma/dy$ a negative quantity. The minus sign in Equation (2.10) makes the positive *dw* consistent with the negative $d\Gamma/dy$.]

The total velocity *w* induced at y_0 by the entire trailing vortex sheet is the summation of Equation (2.10) over all the vortex filaments, that is, the integral of Equation (2.10) from -*b* /2 to *b*/2:

$$\boxed{w(y_0) = -\frac{1}{4\pi}\int_{-b/2}^{b/2} \frac{(d\Gamma/dy)\,dy}{y_0 - y}} \tag{2.11}$$

Equation (2.11) is important in that it gives the value of the downwash at y_0 due to all the trailing vortices.

From Figure 2.3, the induced angle of attack α_i is given by

$$\alpha_i(y_0) = \tan^{-1}\left(\frac{-w(y_0)}{V_\infty}\right) \tag{2.12}$$

Generally, w is much smaller than V_∞, and hence α_i; is a small angle, on the order of a few degrees at most. For small angles, Equation (2.12) yields

$$\alpha_i(y_0) = -\frac{w(y_0)}{V_\infty} \tag{2.13}$$

Substituting Equation (2.11) into (2.12), we obtain

$$\boxed{\alpha_i(y_0) = \frac{1}{4\pi V_\infty}\int_{-b/2}^{b/2}\frac{(d\Gamma/dy)\,dy}{y_0 - y}} \tag{2.14}$$

that is, an expression for the induced angle of attack in terms of the circulation distribution $\Gamma(y)$ along the wing.

Consider again the *effective* angle of attack α_{eff}, as shown in Figure 2.3. Since the downwash varies across the span, then α_{eff} is also variable; $\alpha_{eff} = \alpha_{eff}(y_0)$. The lift coefficient for the airfoil section located at $y = y_0$ is

$$c_l = a_0[\alpha_{eff}(y_0) - \alpha_{L=0}] = 2\pi[\alpha_{eff}(y_0) - \alpha_{L=0}] \tag{2.15}$$

In Equation (2.15), the local section lift slope a_0 has been replaced by the thin airfoil theoretical value of 2π. Also, for a wing with aerodynamic twist, the angle of zero lift $\alpha_{L=0}$ in Equation (2.15) varies with y_0. If there is no aerodynamic twist, $\alpha_{L=0}$ is constant across the span. In any event, $\alpha_{L=0}$ is a known property of the local airfoil sections. From the definition of lift coefficient and from the Kutta-Joukowski theorem, we have, for the local airfoil section located at y_0,

$$L' = \tfrac{1}{2}\rho_\infty V_\infty^2 c(y_0) c_l = \rho_\infty V_\infty \Gamma(y_0) \tag{2.16}$$

From Equation (2.16), we obtain

$$c_l = \frac{2\Gamma(y_0)}{V_\infty c(y_0)} \tag{2.17}$$

Substituting equation (2.17) into (2.15) and solving for α_{eff}, we have

$$\alpha_{eff} = \frac{\Gamma(y_0)}{\pi V_\infty c(y_0)} + \alpha_{L=0} \tag{2.18}$$

We know

$$\alpha_{eff} = \alpha - \alpha_i \tag{2.1}$$

Substituting Equations 2.14, 2.18 into 2.1, we obtain

$$\boxed{\alpha(y_0) = \frac{\Gamma(y_0)}{\pi V_\infty c(y_0)} + \alpha_{L=0}(y_0) + \frac{1}{4\pi V_\infty}\int_{-b/2}^{b/2} \frac{(d\Gamma/dy)\,dy}{y_0 - y}} \tag{2.19}$$

the *fundamental equation of Prandtl 's lifting-line theory;* it simply states that the geometric angle of attack is equal to the sum of the effective angle plus the induced angle of attack. In Equation (2.19), α_{eff} is expressed in terms of Γ, and α_i; is expressed in terms of an integral containing dΓ */dy.* Hence, Equation (2.19) is an integro-differential equation, in which the only unknown is Γ; all the other quantities, α, c,V_∞ and $\alpha_{L=0}$· are known for a finite wing of given design at a given geometric angle of attack in a freestream with given velocity. Thus, a solution of Equation (2.19), yields $\Gamma = \Gamma(y_o)$, where y_o ranges along the span from *-b/2* to *b/2.* The solution $\Gamma = \Gamma(y_0)$ obtained from Equation (2.19) gives us the three main aerodynamic characteristics of a finite wing, as follows:

1. The lift distribution is obtained from the Kutta-Joukowski theorem:

$$L'(y_0) = \rho_\infty V_\infty \Gamma(y_0) \tag{2.20}$$

2. The total lift is obtained by integrating equation 2.20 over the span:

$$L = \int_{-b/2}^{b/2} L'(y)\,dy$$

$$L = \rho_\infty V_\infty \int_{-b/2}^{b/2} \Gamma(y)\,dy \tag{2.21}$$

$$C_L = \frac{L}{q_\infty S} = \frac{2}{V_\infty S}\int_{-b/2}^{b/2} \Gamma(y)\,dy \tag{2.22}$$

3. The induced drag is obtained by inspection of figure 2.3. The induced drag per unit span is

$$D_i' = L_i' \sin\alpha_i$$

Since α_i is small, this relation becomes

$$D_i' = L_i'\alpha_i \tag{2.23}$$

Integrating,

$$D_i = \int_{-b/2}^{b/2} L'(y)\alpha_i(y)\,dy$$

$$D_i = \rho_\infty V_\infty \int_{-b/2}^{b/2} \Gamma(y)\alpha_i(y)\,dy \tag{2.24}$$

The induced drag coefficient is

$$C_{D,i} = \frac{D_i}{q_\infty S} = \frac{2}{V_\infty S}\int_{-b/2}^{b/2} \Gamma(y)\alpha_i(y)\,dy \tag{2.25}$$

Therefore, in Prandtl's lifting-line theory the solution of Equation (2.25) for Γ(y) is clearly the key to obtaining the aerodynamic characteristics of a finite wing.

Elliptic lift distribution:

Consider a circulation distribution given by

$$\Gamma(y) = \Gamma_0 \sqrt{1 - \left(\frac{2y}{b}\right)^2} \tag{2.26}$$

In Equation (2.26), note the following:

1. Γ_0 is the circulation at the origin, as shown in Figure 2.10.
2. The circulation varies elliptically with distance y along the span; hence, it is designated as an *elliptical circulation distribution.* Since $L'(y) = \rho_\infty V_\infty \Gamma(y)$, we also have

$$L'(y) = \rho_\infty V_\infty \Gamma_0 \sqrt{1 - \left(\frac{2y}{b}\right)^2} \tag{2.27}$$

   Hence, we are dealing with an elliptical lift distribution.
3. $\Gamma(b/2) = \Gamma(-b/2) = 0$. Thus, the circulation, hence lift, properly goes to zero at the wing tips, as shown in Figure 2.10.

First, let us calculate the downwash. Differentiating Equation (2.26), we obtain

$$\frac{d\Gamma}{dy} = -\frac{4\Gamma_0}{b^2} \frac{y}{(1 - 4y^2/b^2)^{1/2}} \tag{2.28}$$

Substituting equation 2.28 into 2.11, we have

$$w(y_0) = \frac{\Gamma_0}{\pi b^2} \int_{-b/2}^{b/2} \frac{y}{(1 - 4y^2/b^2)^{1/2}(y_0 - y)} dy \tag{2.29}$$

Substitute

$$y = \frac{b}{2}\cos\theta \qquad dy = -\frac{b}{2}\sin\theta\, d\theta$$

Hence, equation 2.29 becomes

$$w(\theta_0) = -\frac{\Gamma_0}{2\pi b} \int_{\pi}^{0} \frac{\cos\theta}{\cos\theta_0 - \cos\theta} d\theta$$

$$w(\theta_0) = -\frac{\Gamma_0}{2\pi b} \int_{0}^{\pi} \frac{\cos\theta}{\cos\theta - \cos\theta_0} d\theta \tag{2.30}$$

Using standard integration formula as

$$\int_0^\pi \frac{\cos n\theta\, d\theta}{\cos\theta - \cos\theta_0} = \frac{\pi \sin n\theta_0}{\sin\theta_0}$$

Then by n = 1, we get

$$\boxed{w(\theta_0) = -\frac{\Gamma_0}{2b}} \tag{2.31}$$

Which gives downwash is constant over the span for an elliptical lift distribution. For the induced angle of attack,

$$\alpha_i = -\frac{w}{V_\infty} = \frac{\Gamma_0}{2bV_\infty} \tag{2.32}$$

For an elliptic lift distribution, the induced angle of attack is also constant along the span. Note from Equations (2.31) and (2.32) that both the downwash and induced angle of attack go to zero as the wing span becomes infinite. A more useful expression for α_i; can be obtained as follows. Substituting Equation (2.26) into (2.21), we have

$$L = \rho_\infty V_\infty \Gamma_0 \int_{-b/2}^{b/2} \left(1 - \frac{4y^2}{b^2}\right)^{1/2} dy \tag{2.33}$$

Again, using the transformation $y = (b/2)\cos\theta$, equation 2.33 becomes

$$L = \rho_\infty V_\infty \Gamma_0 \frac{b}{2} \int_0^\pi \sin^2\theta \, d\theta = \rho_\infty V_\infty \Gamma_0 \frac{b}{4}\pi \tag{2.34}$$

Solving equation 2.34 for Γ_0,

$$\Gamma_0 = \frac{4L}{\rho_\infty V_\infty b\pi} \tag{2.35}$$

$$\text{However, } L = \tfrac{1}{2}\rho_\infty V_\infty^2 S C_L. \quad , \quad \Gamma_0 = \frac{2V_\infty S C_L}{b\pi} \tag{2.36}$$

Substituting equation 2.36 into 2.32, we obtain

$$\alpha_i = \frac{2V_\infty S C_L}{b\pi} \frac{1}{2bV_\infty}$$

$$\alpha_i = \frac{SC_L}{\pi b^2} \tag{2.37}$$

An important geometric property of a finite wing is the *aspect ratio,* denoted by AR and defined as

$$\text{AR} \equiv \frac{b^2}{S}$$

Hence, Equation (2.37) becomes

$$\boxed{\alpha_i = \frac{C_L}{\pi \text{AR}}} \tag{2.38}$$

Equation (2.38) is a useful expression for the induced angle of attack, as shown below.

The induced drag coefficient is obtained from Equation (2.25), noting that α_i is constant:

$$C_{D,i} = \frac{2\alpha_i}{V_\infty S}\int_{-b/2}^{b/2}\Gamma(y)\,dy = \frac{2\alpha_i\Gamma_0}{V_\infty S}\frac{b}{2}\int_0^\pi \sin^2\theta\,d\theta - \frac{\pi\alpha_i\Gamma_0 b}{2V_\infty S} \tag{2.38a}$$

Substituting equations 2.36 and 2.38 into 2.38a, we obtain

$$C_{D,i} = \frac{\pi b}{2V_\infty S}\left(\frac{C_L}{\pi \mathrm{AR}}\right)\frac{2V_\infty S C_L}{b\pi}$$

$$\boxed{C_{D,i} = \frac{C_L^2}{\pi \mathrm{AR}}} \tag{2.39}$$

Equation (2.39) is an important result. It states that the induced drag coefficient is directly proportional to the square of the lift coefficient. The dependence of induced drag on the lift is not surprising, for the following reason. The induced drag is a consequence of the presence of the wing-tip vortices, which in turn are produced by the difference in pressure between the lower and upper wing surfaces. The lift is produced by this same pressure difference. Hence, induced drag is intimately related to the production of lift on a finite wing; indeed, induced drag is frequently called the *drag due to lift.* Equation (2.39) dramatically illustrates this point. Clearly, an airplane cannot generate lift for free; the induced drag is the price for the generation of lift. The power required from an aircraft engine to overcome the induced drag is simply the power required to generate the lift of the aircraft. Also, note that because $C_{D,i} \propto C_L^2$, the induced drag coefficient increases rapidly as C_L increases and becomes a substantial part of the total drag coefficient when C_L is high (e.g., when the airplane is flying slowly such as on takeoff or landing). Even at relatively high cruising speeds, induced drag is typically 25 percent of the total drag.

Another important aspect of induced drag is evident in Equation (2.39); that is, $C_{D,i}$ is *inversely proportional to aspect ratio.* Hence, to reduce the induced drag, we want a finite wing with the highest possible aspect ratio. Wings with high and low aspect ratios are sketched in Figure 2.11. Unfortunately, the design of very high aspect ratio wings with sufficient structural strength is difficult. Therefore, the aspect ratio of a conventional aircraft is a compromise between conflicting aerodynamic and structural requirements. [It is interesting to note that the aspect ratio of the 1903 Wright Flyer was 6 and that today the aspect ratios of conventional subsonic aircraft range typically from 6 to 8. (Exceptions are the Lockheed U-2 high-altitude reconnaissance aircraft with AR= 14.3 and sailplanes with aspect ratios in the 10 to 22 range.)]

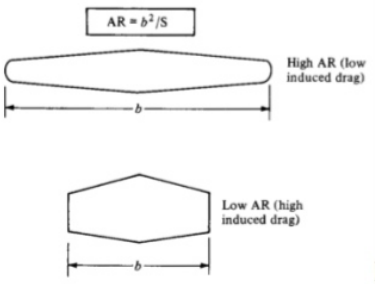

Figure 2.11 High and low aspect ratio wing

Another property of the elliptical lift distribution is as follows. Consider a wing with no geometric twist (i.e., α is constant along the span) and no aerodynamic twist (i.e., $\alpha_{L=0}$ is constant along the span). From Equation (2.38), we have seen that α_i, is constant along the span. Hence, $\alpha_{eff} = \alpha - \alpha_i$; is also constant along the span. Since the local section lift coefficient c_l is given by

$$c_l = a_0(\alpha_{eff} - \alpha_{L=0})$$

then assuming that a_0 is the same for each section ($a_0 = 2\pi$ from thin airfoil theory), c_l must be constant along the span. The lift per unit span is given by

$$L'(y) = q_\infty c c_l \tag{2.40}$$

Solving Equation (2.40) for the chord, we have

$$c(y) = \frac{L'(y)}{q_\infty c_l} \tag{2.41}$$

In Equation (2.41), q_∞ and c_l are constant along the span. However, $L'(y)$ varies elliptically along the span. Thus, Equation (2.41) dictates that for such an elliptic lift distribution, the *chord must vary elliptically along the span;* that is, for the conditions given above, the *wing planform is elliptical.*

The related characteristics-the elliptic lift distribution, the elliptic planform, and the constant downwash-are sketched in Figure 2.12.

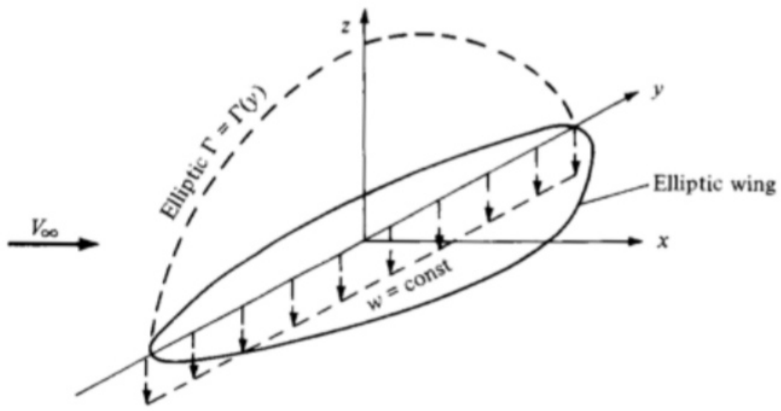

Figure 2.12 Illustration of the related quantities: an elliptic lift distribution, elliptic planform, and constant downwash.

Important formulas:

$$\boxed{C_{D,i} = \frac{C_L^2}{\pi \text{AR}}(1 + \delta)}$$

where $\delta = \sum_2^N n(A_n/A_1)^2$. Note that $\delta \geq 0$; hence, the factor $1 + \delta$ in Equation (5.61) is either greater than 1 or at least equal to 1. Let us define a span efficiency factor, e, as $e = (1 + \delta)^{-1}$. Then Equation (5.61) can be written as

$$\boxed{C_{D,i} = \frac{C_L^2}{\pi e \text{AR}}} \qquad \textbf{[5.62]}$$

where $e \leq 1$. Comparing Equations (5.61) and (5.62) for the general lift distribution with Equation (5.43) for the elliptical lift distribution, note that $\delta = 0$ and $e = 1$ for the elliptical lift distribution. Hence, the lift distribution which yields minimum induced drag is the *elliptical lift distribution*. This is why we have a practical interest in the elliptical lift distribution.

5.3.3 Effect of Aspect Ratio

Returning to Equations (5.61) and (5.62), note that the induced drag coefficient for a finite wing with a general lift distribution is inversely proportional to the aspect ratio, as was discussed earlier in conjunction with the case of the elliptic lift distribution. Note that AR, which typically varies from 6 to 22 for standard subsonic airplanes

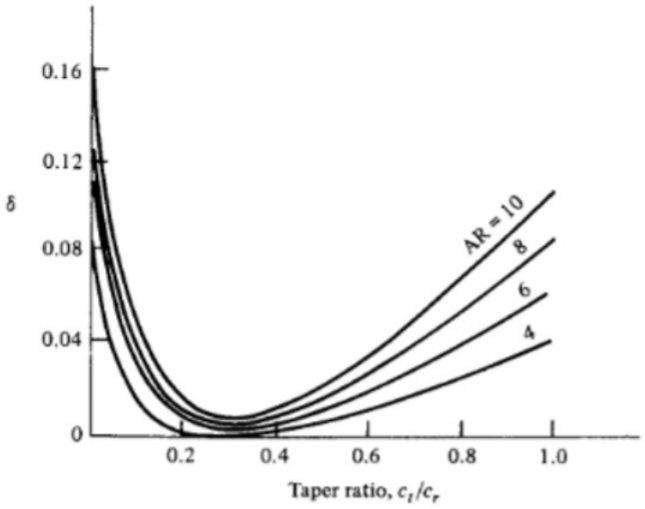

Figure 5.18 Induced drag factor δ as a function of taper ratio. (*Source:* McCormick, B. W., *Aerodynamics, Aeronautics, and Flight Mechanics*, John Wiley & Sons, New York, 1979.)

and sailplanes, has a much stronger effect on $C_{D,i}$ than the value of δ, which from Figure 5.18 varies only by about 10 percent over the practical range of taper ratio. Hence, the primary design factor for minimizing induced drag is not the closeness to an elliptical lift distribution, but rather, the ability to make the aspect ratio as large as possible. The determination that $C_{D,i}$ is inversely proportional to AR was one of the great victories of Prandtl's lifting-line theory. In 1915, Prandtl verified this result with a series of classic experiments wherein the lift and drag of seven rectangular wings with different aspect ratios were measured. The data are given in Figure 5.19. Recall from Equation (5.4), that the total drag of a finite wing is given by

$$C_D = c_d + \frac{C_L^2}{\pi e \text{AR}} \qquad \textbf{[5.63]}$$

and therefore $C_L = c_l$. Assume that we plot C_L for the finite wing versus α_{eff}, as shown at the top of Figure 5.21. Because we are using α_{eff} the lift slope corresponds to that for an infinite wing a_0. However, in real life, our naked eyes cannot see α_{eff}; instead, what we actually observe is a finite wing with a certain angle between the chord line and the relative wind; that is, in practice, we always observe the geometric angle of attack α. Hence, C_L for a finite wing is generally given as a function of α, as sketched at the bottom of Figure 5.21. Since $\alpha > \alpha_{\text{eff}}$, the bottom abscissa is stretched, and hence the bottom lift curve is less inclined; it has a slope equal to a, and Figure 5.21 clearly shows that $a < a_0$. The effect of a finite wing is to *reduce* the lift slope. Also, recall that at zero lift, there are no induced effects; i.e., $\alpha_i = C_{D,i} = 0$. Thus, when $C_L = 0$, $\alpha = \alpha_{\text{eff}}$. As a result, $\alpha_{L=0}$ is the same for the finite and the infinite wings, as shown in Figure 5.21.

The values of a_0 and a are related as follows. From the top of Figure 5.21,

$$\frac{dC_L}{d(\alpha - \alpha_i)} = a_0$$

Integrating, we find

$$C_L = a_0(\alpha - \alpha_i) + \text{const} \qquad \textbf{[5.67]}$$

Substituting Equation (5.42) into (5.67), we obtain

$$C_L = a_0\left(\alpha - \frac{C_L}{\pi \text{AR}}\right) + \text{const} \qquad \textbf{[5.68]}$$

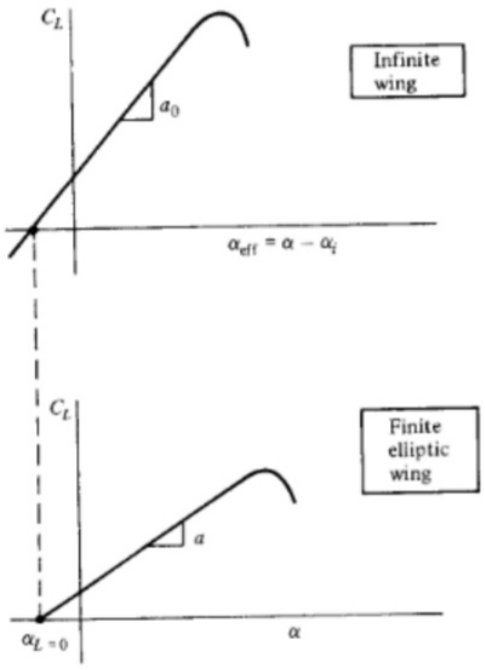

Figure 5.21 Lift curves for an infinite wing versus a finite elliptic wing.

Differentiating Equation (5.68) with respect to α, and solving for $dC_L/d\alpha$, we obtain

$$\frac{dC_L}{d\alpha} = a = \frac{a_0}{1 + a_0/\pi \text{AR}} \qquad \textbf{[5.69]}$$

Equation (5.69) gives the desired relation between a_0 and a for an elliptic finite wing. For a finite wing of general planform, Equation (5.69) is slightly modified, as given below:

$$a = \frac{a_0}{1 + (a_0/\pi \mathrm{AR})(1 + \tau)} \qquad \textbf{[5.70]}$$

In Equation (5.70), τ is a function of the Fourier coefficients A_n. Values of τ were first calculated by Glauert in the early 1920s and were published in Reference 18, which should be consulted for more details. Values of τ typically range between 0.05 and 0.25.

Extended lifting line theory – Lifting surface theory, Vortex Lattice method for wings

Prandtl's classical lifting-line theory gives reasonable results for straight wings at moderate to high aspect ratio. However, for low-aspect-ratio straight wings, swept wings, and delta wings, classical lifting-line theory is inappropriate. For such planforms, sketched in Figure 5.30,

Here, a simple lifting line spans the wing, with its associated trailing vortices. The circulation Γ varies with y along the lifting line. Let us extend this model by placing a *series* of lifting lines on the plane of the wing, at different chordwise stations; that is, consider a large number of lifting lines all parallel to the y axis, located at different values of x, as shown in Figure **2.10** In the limit of an infinite number of lines of infinitesimal strength, we obtain a vortex sheet, where the vortex lines run parallel to the y axis. The strength of this sheet (per unit length in the x direction) is denoted by γ, where γ varies in the y direction, analogous to the variation of Γ for the single lifting line in Figure 5.13. Moreover, each lifting line will have, in general, a different overall strength, so that γ varies with x also. Hence, $\gamma = \gamma(x, y)$ as shown in Figure 5.31. In addition, recall that each lifting line has a system of trailing vortices; hence, the series of lifting lines is crossed

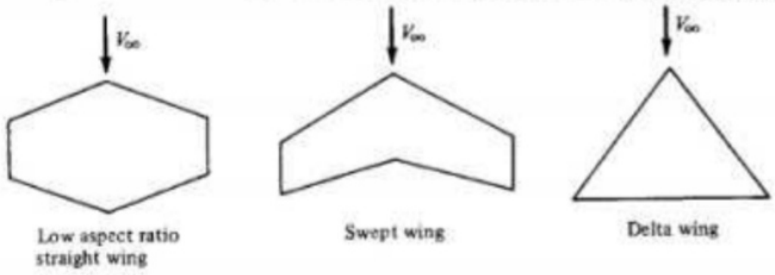

Figure 5.30 Types of wing planforms for which classical lifting-line theory is not appropriate.

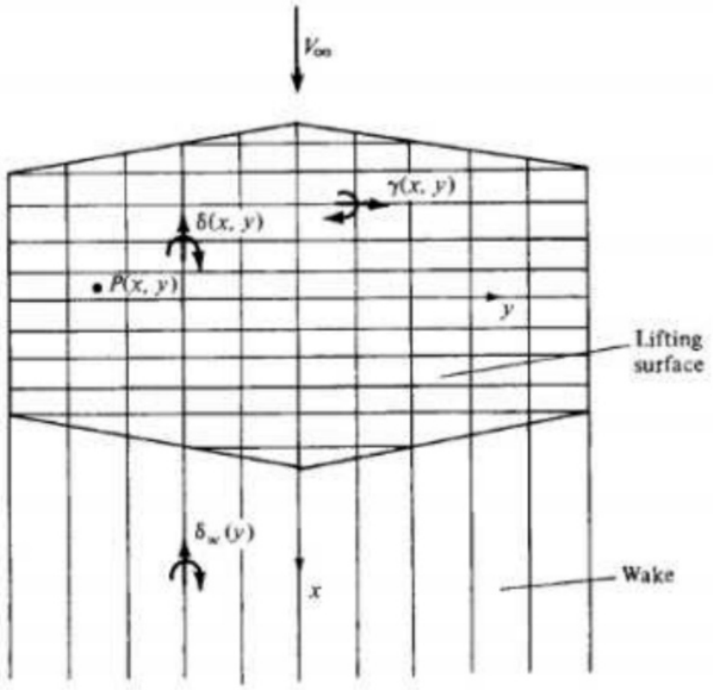

Figure 5.31 Schematic of a lifting surface.

by a series of superimposed trailing vortices parallel to the x axis. In the limit of an infinite number of infinitesimally weak vortices, these trailing vortices form another vortex sheet of strength δ (per unit length in the y direction).

To see this more clearly, consider a single line parallel to the x axis. As we move along this line from the leading edge to the trailing edge, we pick up an additional superimposed trailing vortex each time we cross a lifting line. Hence, δ must vary with x. Moreover, the trailing vortices are simply parts of the horseshoe vortex systems, the leading edges of which make up the various lifting lines. Since the circulation about each lifting line varies in the y direction, the strengths of different trailing vortices will, in general, be different. Hence, δ also varies in the y direction, that is, $\delta = \delta(x, y)$, as shown in Figure 5.31. The two vortex sheets—the one with vortex lines running parallel to y with strength γ (per unit length in the x direction) and the other with vortex lines running parallel to x with strength δ (per unit length in the y direction)—result in a *lifting surface* distributed over the entire planform of the wing, as shown in Figure 5.31. At any given point on the surface, the strength of the lifting surface is given by both γ and δ, which are functions of x and y. We denote $\gamma = \gamma(x, y)$ as the spanwise vortex strength distribution and $\delta = \delta(x, y)$ as the chordwise vortex strength distribution.

Note that downstream of the trailing edge we have no spanwise vortex lines, only trailing vortices. Hence, the wake consists of only chordwise vortices. The strength of this wake vortex sheet is given by δ_w (per unit length in the y direction). Since in the wake the trailing vortices do not cross any vortex lines, the strength of any given trailing vortex is constant with x. Hence, δ_w depends only on y and, throughout the wake, $\delta_w(y)$ is equal to its value at the trailing edge.

Consider point P located at (x, y) on the wing, as shown in Figure 5.31. The lifting surface and the wake vortex sheet both induce a normal component of velocity at point P. Denote this normal velocity by $w(x, y)$. We want the wing planform to be a stream surface of the flow; that is, we want the sum of the induced $w(x, y)$ and the normal component of the freestream velocity to be zero at point P and for all points on the wing—this is the flow-tangency condition on the wing surface.

The central theme of lifting-surface theory is to find $\gamma(x, y)$ and $\delta(x, y)$ such that the flow-tangency condition is satisfied at all points on the wing. [Recall that in the wake, $\delta_w(y)$ is fixed by the trailing-edge values of $\delta(x, y)$; hence, $\delta_w(y)$ is not, strictly speaking, one of the unknown dependent variables.]

Let us obtain an expression for the induced normal velocity $w(x, y)$ in terms of γ, δ, and δ_w. Consider the sketch given in Figure 5.32, which shows a portion of the planview of a finite wing. Consider the point given by the coordinates (ξ, η). At this point, the spanwise vortex strength is $\gamma(\xi, \eta)$. Consider a thin ribbon, or filament, of the spanwise vortex sheet of incremental length $d\xi$ in the x direction. Hence, the strength of this filament is $\gamma\, d\xi$, and the filament stretches in the y (or η) direction. Also, consider point P located at (x, y) and removed a distance r from the point (ξ, η). From the Biot-Savart law, Equation **2.2**, the incremental velocity induced at P by a segment $d\eta$ of this vortex filament of strength $\gamma\, d\xi$ is

$$|\mathbf{dV}| = \left| \frac{\Gamma}{4\pi} \frac{\mathbf{dl} \times \mathbf{x}}{|\mathbf{r}|^3} \right| = \frac{\gamma\, d\xi}{4\pi} \frac{(d\eta) r \sin\theta}{r^3} \qquad \textbf{[5.77]}$$

Examining Figure 5.32, and following the right-hand rule for the strength γ, note that $|\mathbf{dV}|$ is induced downward, into the plane of the wing (i.e., in the negative z direction). Following the usual sign convention that w is positive in the upward direction (i.e., in the positive z direction), we denote the contribution of Equation (5.77) to the induced velocity w as $(dw)_\gamma = -|\mathbf{dV}|$. Also, note that $\sin\theta = (x - \xi)/r$. Hence, Equation (5.77) becomes

$$(dw)_\gamma = -\frac{\gamma}{4\pi}\frac{(x-\xi)d\xi\,d\eta}{r^3} \qquad \textbf{[5.78]}$$

Considering the contribution of the elemental chordwise vortex of strength $\delta\,d\eta$ to the induced velocity at P, we find by an analogous argument that

$$(dw)_\delta = -\frac{\delta}{4\pi}\frac{(y-\eta)d\xi\,d\eta}{r^3} \qquad \textbf{[5.79]}$$

To obtain the velocity induced at P by the entire lifting surface, Equations (5.78) and (5.79) must be integrated over the wing planform, designated as region S in Figure 5.32. Moreover, the velocity induced at P by the complete wake is given by an equation analogous to Equation (5.79), but with δ_w instead of δ, and integrated over the wake, designated as region W in Figure 5.32. Noting that

$$r = \sqrt{(x-\xi)^2 + (y-\eta)^2}$$

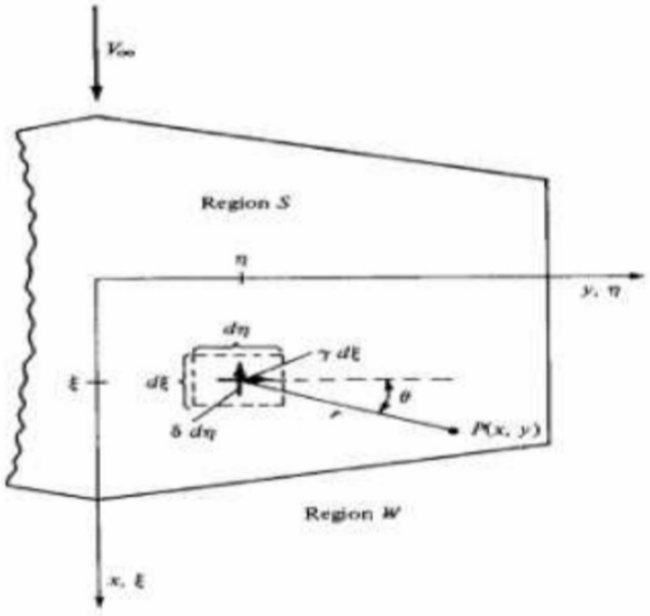

Figure 5.32 Velocity induced at point P by an infinitesimal segment of the lifting surface. The velocity is perpendicular to the plane of the paper.

the normal velocity induced at P by both the lifting surface and the wake is

$$w(x,y) = -\frac{1}{4\pi}\iint_S \frac{(x-\xi)\gamma(\xi,\eta) + (y-\eta)\delta(\xi,\eta)}{[(x-\xi)^2 + (y-\eta)^2]^{3/2}}d\xi\,d\eta - \frac{1}{4\pi}\iint_W \frac{(y-\eta)\delta_w(\xi,\eta)}{[(x-\xi)^2 + (y-\eta)^2]^{3/2}}d\xi\,d\eta \qquad \textbf{[5.80]}$$

The central problem of lifting-surface theory is to solve Equation (5.80) for $\gamma(\xi, \eta)$ and $\delta(\xi, \eta)$ such that the sum of $w(x, y)$ and the normal component of the freestream is zero, that is, such that the flow is tangent to the planform surface S. The details of various lifting-surface solutions are beyond the scope of this book; rather, our purpose here was simply to present the flavor of the basic model.

On each panel, either constant or prescribed variations of both γ and δ can be made. Control points on the panels can be chosen, where the net normal flow velocity is zero. The evaluation of equations like Equation (5.80) at these control points results in a system of simultaneous algebraic equations that can be solved for the values of the γ's and δ's on all the panels.

A related but somewhat simpler approach is to superimpose a finite number of horseshoe vortices of different strengths Γ_n on the wing surface. For example, consider Figure 5.33, which shows part of a finite wing. The dashed lines define a panel on the wing planform, where l is the length of the panel in the flow direction. The panel is a trapezoid; it does not have to be a square, or even a rectangle. A horseshoe vortex *abcd* of strength Γ_n is placed on the panel such that the segment *bc* is a distance $l/4$ from the front of the panel. A control point is placed on the

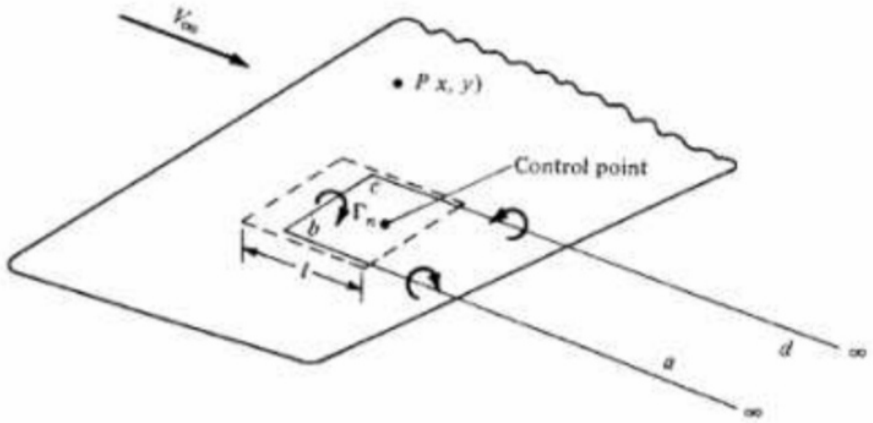

Figure 5.33 Schematic of a single horseshoe vortex, which is part of a vortex system on the wing.

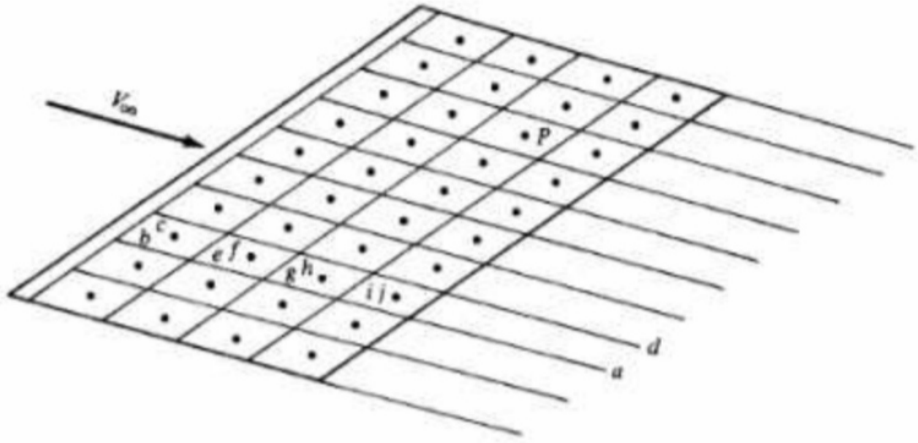

Figure 5.34 Vortex lattice system on a finite wing.

centerline of the panel at a distance $\frac{3}{4}l$ from the front. The velocity induced at an arbitrary point P only by the single horseshoe vortex can be calculated from the Biot-Savart law by treating each of the vortex filaments *ab*, *bc*, and *cd* separately. Now consider the entire wing covered by a finite number of panels, as sketched in Figure 5.34. A series of horseshoe vortices is now superimposed. For example, on one panel at the leading edge, we have the horseshoe vortex *abcd*. On the panel behind it, we have the horseshoe vortex *aefd*. On the next panel, we have *aghd*, and on the next, *aijd*, etc. The entire wing is covered by this lattice of horseshoe vortices, each of different unknown strength Γ_n. At any control point P, the normal velocity induced by *all* the horseshoe vortices can be obtained from the Biot-Savart law. When the flow-tangency condition is applied at all the control points, a system of simultaneous algebraic equations results which can be solved for the unknown Γ_n's. This numerical approach is called the *vortex lattice method* and is in wide use today for the analysis of finite-wing properties.